Characterization of Subgrains for Ferritic Heat-Resisting Steels with Different Creep-Fatigue Susceptibility

Masao Hayakawa, Megumi Kimura, Kazuo Kobayashi
Materials Reliability Center, National Institute for Materials Science(NIMS)
1-2-1 Sengen, Tsukuba, Ibaraki, Japan

A new observation method was developed for visualizing subgrains on the chemical-mechanically polished surface of ferritic heat-resisting steels, using field emission-type (FE) SEM. The backscattered electron images revealed clearly visualized subgrain structures that were not influenced by the presence of precipitated particles.

The authors then investigated the use of FE-backscattered electron images to visualize low-angle boundaries such as subgrain boundaries. The specimen surface must be free of any strain or unevenness, so in this study the authors adopted the new technique of chemical mechanical polishing, which involves the simultaneous application of chemical corrosion and mechanical polishing to prepare specimen surfaces for structural observation.

In this study, subgrains of ferritic heat-resisting steels were quantified based on the microstructural observation. In particular, we focused on differences in the distributions of subgrains for two types of 12Cr-2W steels with different creep-fatigue susceptibility and investigate the relationships between creep-fatigue properties and changes in subgrains.

Keywords: Heat-resisting ferritic steel, Creep-fatigue, Martensite block, Subgrain, Grain boundary precipitates

1. Introduction

Heat-resisting ferritic steels with high-chromium content have high tensile strengths at high temperatures and small coefficients of thermal expansion as compared with austenite stainless steels. A tungsten-strengthened 12 mass% Cr and 2 mass% W ferritic steel has recently been developed and is presently in use for main steam pipes and headers in power plants [1]. These steels must satisfy the required creep-fatigue properties as well as the required creep strength.

The authors evaluated the creep properties and creep-fatigue properties for 9-12 % Cr and 2-3 % W ferritic steels in a previous study [2]. The study showed that steels that had higher strength and higher creep ductility had longer creep-fatigue lives. The authors also found that steels with short creep-fatigue lives fractured along prior austenite grain boundaries, while steels with long creep-fatigue lives fractured from inside of the grains.

Heat-resisting ferritic steels with high tensile strengths have tempered martensitic structures, as shown in the optical microscopic photograph in Fig. 1(a) [3-5]. The authors found that this complicated tempered martensitic structure has a stratified structure, as shown in Fig.1(b), by performing secondary electron image observations, using field-emission-type scanning electron microscopy (FE-SEM), of a specimen whose surface had been polished using a special electrolytic

method; and transmission electron microscopic (TEM) observation of thin-film specimens [5]. As shown in the schematic diagram, the structure was composed of constituents that differed in size, of which prior austenite (γ) grains are the largest, followed, in descending order of size, by packets, blocks, and subgrains. The authors call this structure a "multi-scale" structure [5].

Prior γ grain boundaries, packet boundaries and block boundaries are high-angle boundaries, and thus create slight irregularities in the surface that reveal differences in crystal orientation when the surface is polished using a special electrolytic method [5-7]. The multi-scale structure of these boundaries was clearly visualized by observing the specimen surface using the secondary electrons generated by high-resolution FE-SEM.

On the other hand, subgrain boundaries have low misorientation angles, and electropolished surfaces did not show any unevenness attributable to subgrain boundaries, making it impossible to observe the subgrain structure by means of FE-SEM secondary electrons. The subgrain structure can be visualized by TEM observation; however, TEM has the demerit of requiring thin-film samples to be prepared, and suffers from a small range and limited field of observation.

The authors then investigated the use of FE-SEM backscattered electron images to visualize low-angle boundaries such as subgrain boundaries. The specimen surface must be free of any strain or unevenness [8,9], so in this study the authors adopted the new technique of chemical mechanical polishing (CMP) [8,9], which involves the simultaneous application of chemical corrosion and mechanical polishing to prepare specimen surfaces for structural observation.

In this study, distributions of subgrains and precipitates on grain boundaries were quantitatively evaluated for two types of 12Cr-2W steels subjected to creep-fatigue tests [2]. One of the steels had a short fatigue life, showed grain boundary fractures, and was formed into a main steam pipe (ASTM-SA355-P122, hereinafter referred to as “pipe steel”). The other had a long fatigue life, showed transgranular fractures, and was formed into a plate (hereinafter referred to as “plate steel”).

This study focused on evaluating the distributions of subgrains and grain boundary precipitates to enable characterization of the relationship between microstructures and creep-fatigue properties in ferritic steels.

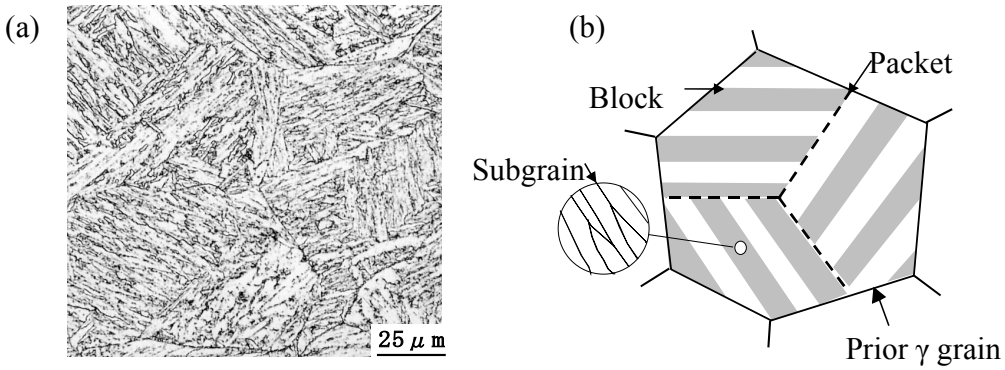

Fig.1 Optical micrograph (a) and schematic drawing (b) of the construction of the multi-scale structure within a prior austenite (γ) grain for ferritic 12Cr-2W steel.

2. Experimental procedure

2.1 Material information

The chemical compositions of the specimens and the thermal treatment conditions are shown in Tables 1(a) and (b), respectively. Their tensile strengths showed the same value of 285 MPa at 923 K. The creep-fatigue test was conducted under a 923 K atmosphere, using tensile strain trapezoidal waves (strain-holding duration 10.8 ks), by controlling the axial strain, and maintaining the total strain range of 1.0 %. The fatigue lives of the pipe and plate steels were different at 309 and 568 cycles, respectively [2]. Ferritic steels prepared under these thermal treatment conditions have lath martensite structures, the formation of which is hierarchic in the order of smaller size, laths, blocks, packets, and prior austenite grains [5]. The average grain sizes of the prior austenite grains of the pipe and plate materials were about 150-200 μm and 30 μm, respectively.

Table 1 Chemical compositions and thermal processing of the pipe and plate materials in (a) and (b), respectively.

(a)Chemical compositions of the materials used in this study (mass%).

Material	Form	C	Si	Mn	Cu	Ni	Cr	W	Mo	V	Nb	N	Fe
12Cr-2W	Pipe	0.14	0.26	0.65	0.74	0.4	11.03	1.95	0.29	0.2	0.07	0.06	Bal.
12Cr-2W	Plate	0.12	0.28	0.63	0.98	0.35	10.7	1.9	0.36	0.22	0.06	0.076	Bal.

(b)Thermal processing of the materials used in this study.

Material	Form	Normalizing		Tempering	
12Cr-2W	Pipe	1323 K, 3.6 ks	Air cooled	1053 K, 21.6 ks	Air cooled
12Cr-2W	Plate	1323 K, 6.12 ks	Air cooled	1043 K, 21.6 ks	Air cooled

2.2 Specimen preparation

Thin sections 7 mm in length, 5 mm in width and 1 mm in thickness were excised and subjected to the following treatments for TEM and FE-SEM observation.

(1) Specimen for subgrain observation by TEM

The sections were mechanically polished to a thickness of approximately 70 μm, and were then electrolytically polished using the Twin-Jet method and a solvent containing 5vol.% perchloric acid and 95vol.% acetic acid.

TEM observation was performed at an acceleration voltage of 200 kV.

(2) Specimens with high-angle boundaries and observation of precipitates by FE-SEM

The observation surfaces were polished to a mirror finish with diamond particles 1 μm in diameter, and then finished by electropolishing at 273 K using a solvent containing 8vol.% perchloric acid, 10vol.% butoxyethanol, 70vol.% ethanol and 12vol.% distilled water, while applying a voltage of 40 V for 10 s.

Secondary electron FE-SEM images were obtained at a working distance of 10 mm and an accelerating voltage of 15 kV.

(3) Specimen for subgrain observation by FE-SEM

Specimens were immersed in 500 cm3 of an aqueous solution that contained 200 g of silica micro powder in a container with an abrasive cloth attached to the bottom. The pressure between the specimens and the abrasive disk was set at about 10 kPa, and the abrasive disk was slowly rotated at a speed of 1 rps for 1.8

ks. An abrasion period shorter than 1.8 ks resulted in an uneven specimen surface. The smoothing of single-crystal materials such as semiconductors depends only on time, with the correct duration of processing creating the required smooth surfaces. However, the surfaces of ferritic steels corrode if polished for too long.

Backscattered electron FE-SEM images were obtained at a working distance of 7 mm and an accelerating voltage of 5 kV.

3. Results and discussion

3.1 Microstructures of grain boundary precipitates

Figs.2(a) and (b) show, respectively, the FE-SEM images of the pipe and plate materials before the creep-fatigue test. The images show segregation of precipitates on block boundaries as well as prior austenite grain boundaries. The blocks in the pipe steel, which had larger prior γ grains than those in the plate material, were longer than those in the plate material.

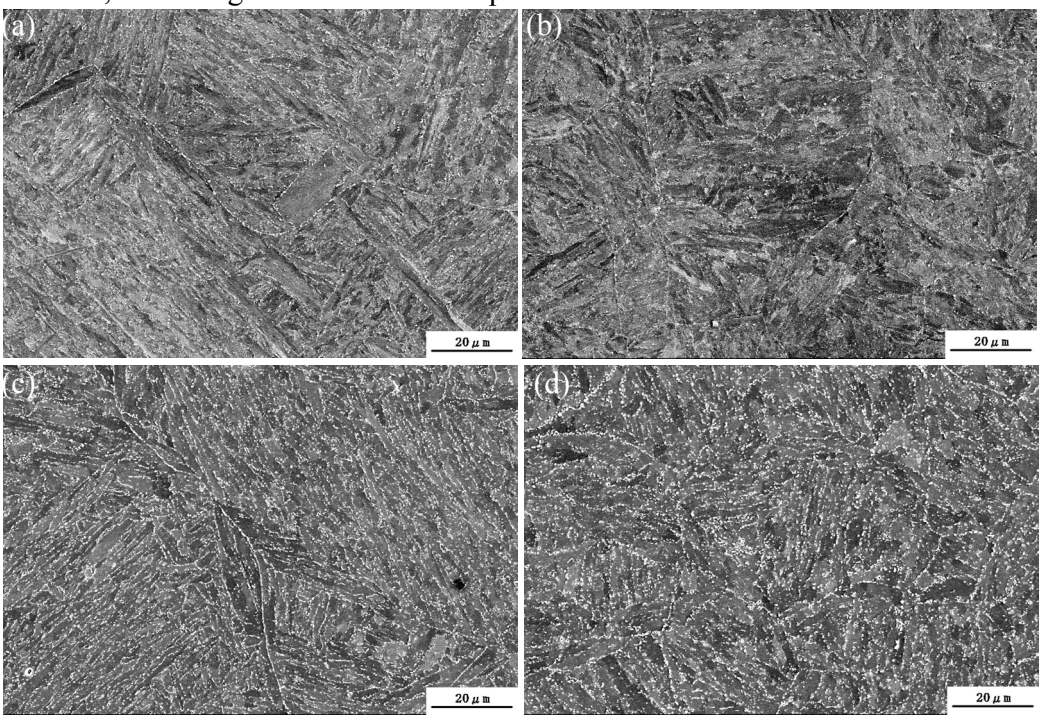

Fig.2 FE-scanning electron images of the electropolished surfaces for the pipe and plate materials before the creep-fatigue testing in (a) and (b), respectively, and for the pipe and plate materials after the testing in (c) and (d).

Figs.2(c) and (d) show FE-SEM images of the pipe and plate steels after the creep-fatigue testing. The creep-fatigue test up to rupture causes no change in block size for both the materials. The mean block widths before and after the testing were the same values of 1.5 μm for the both materials.

The images show larger and denser precipitates on the prior γ grain boundaries and block boundaries after the test than beforehand. $Cr_{23}C_6$ and Fe_2W (Laves phase) have been shown to precipitate on Cr-W steels [10] and relationships between $Cr_{23}C_6$ and creep properties have been controversial [11].

In the pipe material, the precipitates accumulated densely on the prior austenite grain boundaries, showing no breaks. The plate material, on the other hand, showed grain boundary precipitates larger than those in the pipe material, but intervals were more frequently observed. This suggests that the distribution of precipitates, i.e. occupancy (or cover ratio) of precipitates on the prior γ grain boundaries differed between the steels. The percentage of the area covered with precipitates on the prior γ grain boundaries *f*g (=Σ(*l*g/*L*g)x100%) was determined for each FE-SEM image (x 5,000). *l*g is the length of precipitates along the prior γ grain boundary, and *L*g is the length of the boundary [5].

Before the test, the mean length of the grain boundary precipitate was 273 nm for the pipe material, larger than that of the plate material at 212 nm. After the test, the mean length was 337 nm for the pipe material, smaller than that of the plate material at 376 nm. The precipitates did not grow appreciably on the pipe material, which has a short creep-fatigue life and fractured earlier, while the precipitates on the plate material, which has a long creep-fatigue life, continued to grow.

Before the test, the distribution of the occupancy fluctuated more in the pipe material than in the plate material, but the mean occupancy of the pipe and plate materials were 52% and 47%, respectively, showing no difference. After the test, the occupancy of the pipe material on the grain boundary was over 55% in all images, with a high mean of 69%. On the other hand, the occupancy of the plate material on the grain boundary ranged from 45 to 65%, and the mean was only 57%. The significant difference was likely to be attributable to the small size of the prior γ grains in the plate steel, which was only 1/5 of the size of the grains in the pipe steel. The small size resulted in an increased grain boundary area per unit volume of the plate material and thus a reduced frequency of precipitate segregation per unit grain boundary length.

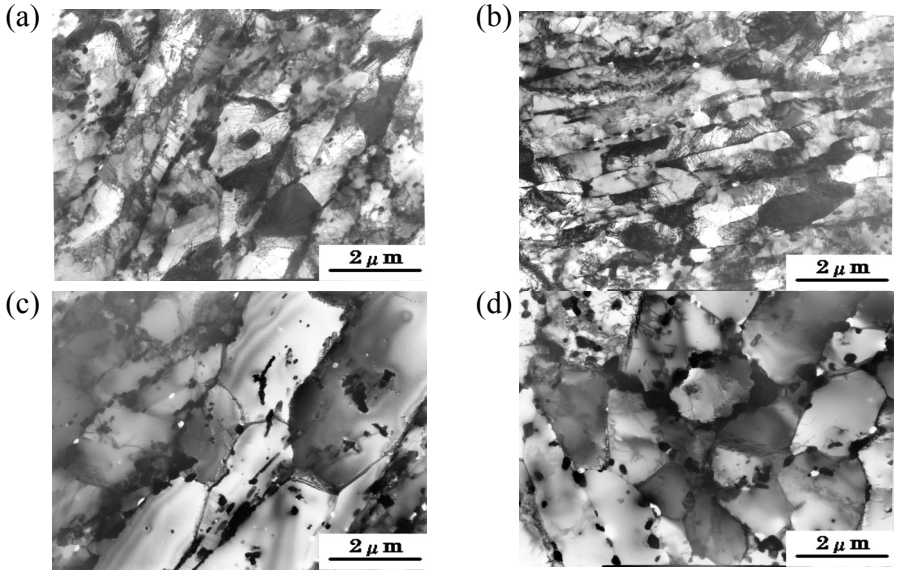

Fig.3 TEM images for the pipe and plate materials before the creep-fatigue test in panels (a) and (b), respectively, and for the pipe and plate materials after the testing in (c) and (d).

3.2 Subgrain structures

The TEM images of the pipe and plate materials before and after the creep-fatigue tests are shown in Figs.3. Before the test, it was difficult to identify precipitates, since the dislocation density was too high. As in the sizes of prior γ grains, the lath width was larger in the pipe material than in the plate material.

After the test, subgrains which crossed over several laths were observed. The dislocation density within the subgrains decreased, and the subgrain boundary precipitates were larger than before the test. The size of each subgrain corresponds to the block width (1 to 2 μm) in the SEM images. Since there were many precipitates on the block boundaries in the SEM images, many precipitates were observed on the subgrain boundaries in the TEM images.

The plate material showed isometric subgrains. On the other hand, the pipe material showed many coarse subgrains with an elongated axis. In the pipe material, which had large prior γ grain sizes and long parallel laths, it is possible that elongated subgrains formed that crossed several parallel laths.

Figs.4 show low- and high-magnification of FE-backscattered electron images of the CMP surface for the pipe in (a) and (b), and plate materials in (c) and (d), before the creep-fatigue testing, respectively. Since the surface is smooth, precipitate particles, which were minute, could not resolved. Therefore, the effects of the precipitates were removed: and the subgrain structures are isolated and appear in black-and-white contrast. Since FE-SEM has a larger visual field than TEM for taking subgrain structure images, the FE-SEM backscattered electron images enabled coarse subgrains over 1 μm in width and fine subgrains in a single field to be identified simultaneously.

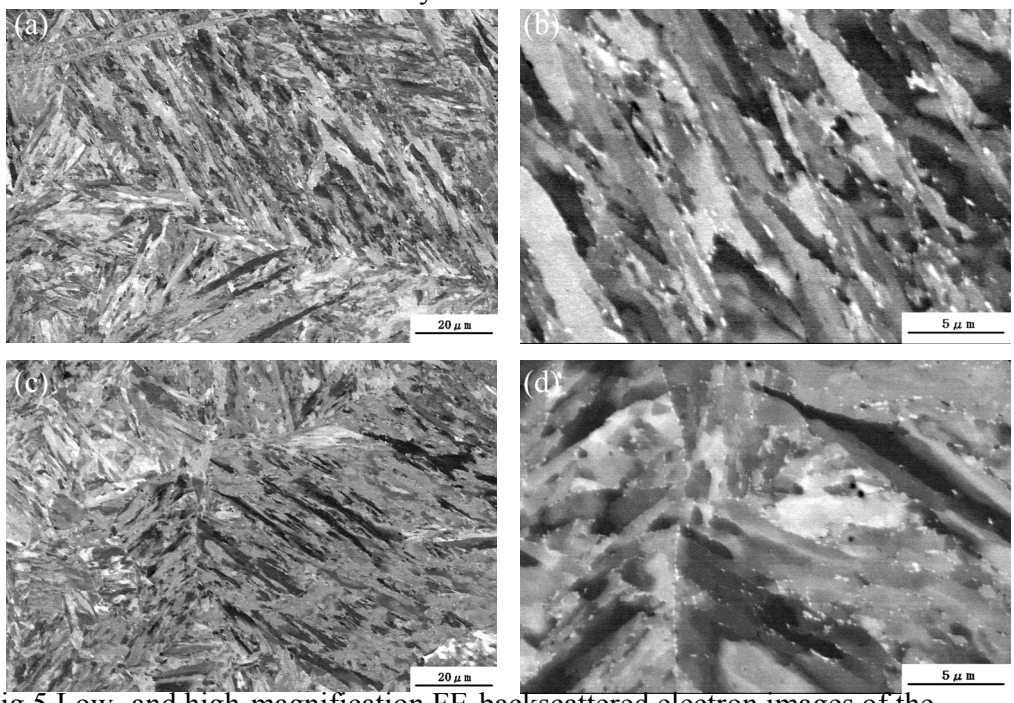

Fig.5 Low- and high-magnification FE-backscattered electron images of the chemical mechanically polished surface for the pipe in (a) and (b), and plate materials in (c) and (d) before the creep-fatigue testing, respectively.

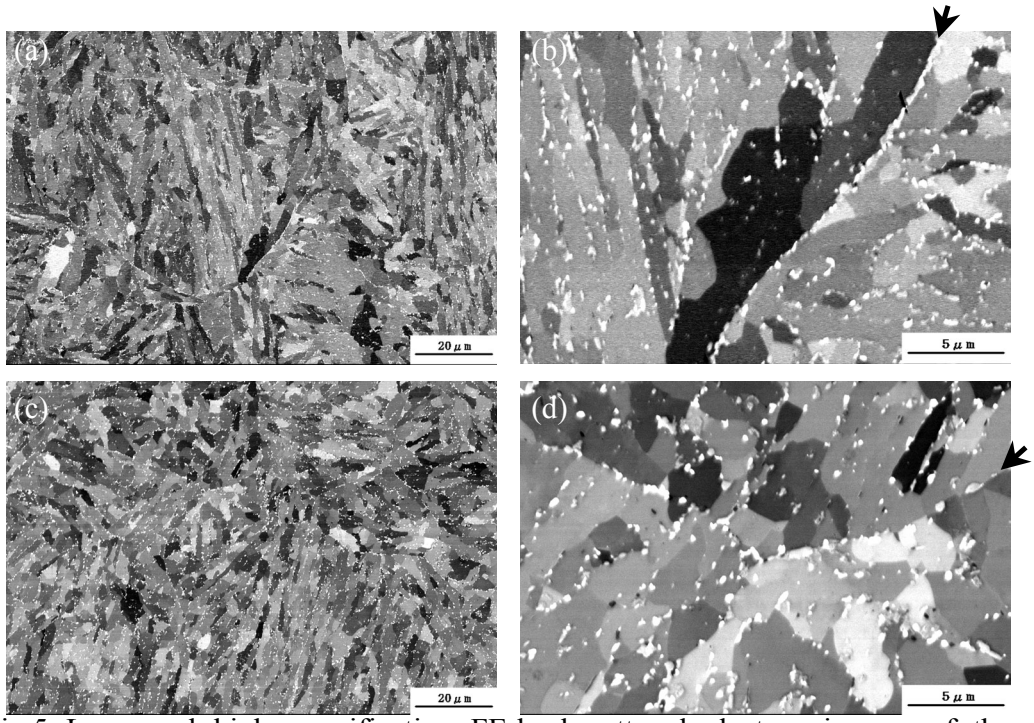

Fig.5 Low- and high-magnification FE-backscattered electron images of the chemical mechanically polished surface for the pipe in (a) and (b), and plate materials in (c) and (d) after the creep-fatigue testing, respectively. Prior γ grain boundaries are indicated by arrows.

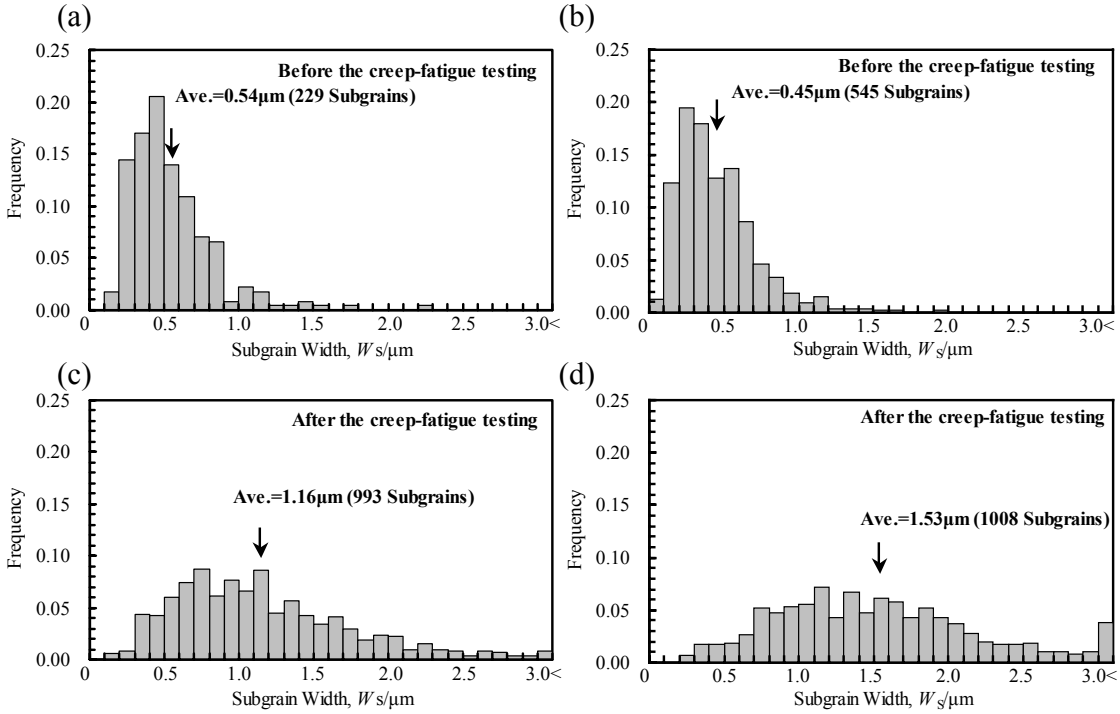

Fig.6 The frequency of the subgrain size is shown as the function of width. Width were measured in high-magnification backscattered images for pipe in (a) and (b), respectively, and plate in (c) and (d) before and after the creep-fatigue testing.

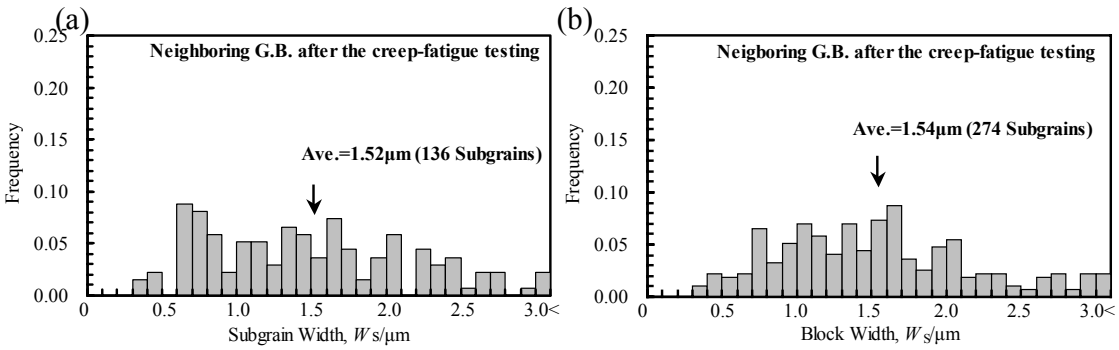

Fig.6 The frequency of the subgrain size neighboring prior γ grain boundaries is shown as the function of width. Width were measured in high-magnification backscattered images for pipe and plate materials in (a) and (b) after the creep-fatigue testing, respectively.

Figs.5 show low- and high-magnification of FE-backscattered electron images of the CMP surface for the pipe in (a) and (b), and plate materials in (c) and (d), after the creep-fatigue testing, respectively. Fig.6 are histograms of subgrain widths determined from several backscattered electron images of the CMP surface. The mean subgrain width was approximately 0.5 μm for the both materials before the creep-fatigue testing, very similar to the value determined using the TEM images. Therefore, the subgrain structure obtained from the backscattered electron image of the CMP surface was concluded to agree with the subgrain structure identified in the TEM images [9].

After the testing, the mean subgrain width for the pipe material was 1.2 μm, while that for the plate material was 1.5 μm corresponding to the block width, which has long creep-fatigue life. The mean subgrain width neighboring prior γ grain boundaries, as shown in Figs.6, that for the pipe was 1.5 μm, then those subgrains became coarse in local than that interior grain. The pipe materials had the short fatigue life, showed grain boundary fractures On the other hand, for the plate which showed transgranular fractures, the mean values interior and neighboring prior γ grain boundaries were the same values of 1.5 μm, subgrain became uniformly coarse over the microstructure.

3.3 Relationship between microstructures and creep-fatigue properties

The pipe material, which had a creep-fatigue life of only 309 cycles and showed intergranular boundary fractures, had a high grain boundary precipitate occupancy of 69%. On the other hand, the plate material, which had a long creep-fatigue life of 568 cycles and showed transgranular fractures, had a lower grain boundary precipitate occupancy of only 57%. In the pipe material, the grain boundary precipitates were densely formed at smaller intervals. It is considered that as the occupation area of precipitates on prior γ grain boundaries increases and subgrain near the grain boundaries became locally corase, the resistance of prior γ grain boundary fractures decreases, and the number of dislocations piled up at the precipitates, which causes stress concentration, increases. On the other hand, the plate material had low boundary occupancy and isometric subgrains of

relatively uniform size, resulting in uniform plastic deformation overall, with little concentration of stress at prior γ grain boundaries.

4. Conclusions

Statistical estimation of subgrain sizes and distribution is an important technique for predicting the creep or creep-fatigue properties of ferritic steels, since subgrain sizes are markedly changed by dislocation recovery during creep or creep-fatigue. The observation method developed in this study, which enables easy statistical evaluation of subgrain structures for the pipe and plate materials, which were heat-resisting 12Cr-2W ferritic steels of the same chemical compositions and tensile strength but with different creep-fatigue properties. The difference in creep-fatigue lives between the pipe and plate materials could be explained in terms of the differences in subgrains and occupancy of precipitates on grain boundaries.

References

[1] F. Masuyama, in: E. Metcalfe (Eds.), EPRI/National Power Conf. on New Steels for Advanced Plant up to 620ºC, Soc. Chem. Indus., London, 1995, p.98.
[2] M. Kimura, K. Kobayashi, K. Yamaguchi, Mater. Sci. Res. Inter. 9 (2003) 50.
[3] G. Krauss, C.J. McMahon Jr., in: G.B. Olson, W.S. Owen (Eds.), Martensite, ASM International, New York, 1992, p.295.
[4] A.R. Marder, G. Krauss, Trans. ASM 60 (1967) 651.
[5] M. Hayakawa, K. Yamaguchi, M. Kimura, K. Kobayashi, Mater. Trans. 45 (2004) 3291.
[6] M. Hayakawa, S. Matsuoka, K. Tsuzaki, Mater. Trans. 43 (2002) 1758.
[7] M. Hayakawa, S. Matsuoka, K. Tsuzaki, H. Hanada, M. Sugisaki, Scripta Mater. 47 (2002) 655.
[8] M. Hayakawa, K. Yamaguchi, M. Kimura, K. Kobayashi, Mater. Let. 58 (2004) 2565.
[9] M. Hayakawa, S. Matsuoka, Y. Furuya, Y. Ono, Mater. Trans. 46 (2005) 2443.
[10] F. Abe, H. Araki, T. Noda, Metall. Trans. A 22A (1991) 2225.
[11] F. Abe, S. Nakazawa, Metall. Trans. A 23A (1992) 3025.